Recent results with the Los Alamos Constant-Q Spectrometer

M. Yethiraj and R. A. Robinson
Los Alamos Neutron Scattering Center
Los Alamos National Laboratory
Los Alamos, New Mexico 87545
USA

1. Introduction

The Constant-Q geometry for measuring collective excitations on pulsed-neutron sources was proposed and tested by Windsor et al.,[1] in 1978. By 1985, a second improved Constant-Q spectrometer had been built at Los Alamos[2], and improvements over Windsor's version were listed in a previous ICANS proceedings[3]. In this article, we list further improvements made to the Los Alamos spectrometer and give a brief account of other progress on it.

2. Improvements since 1985

(a) Following the flight-path nomenclature in Ref. 2, L_2 was increased from 200 mm to 400 mm. This was made possible with the large multi-element analysers described elsewhere in these proceedings[4]. It had effect in reducing backgrounds and diminishing contamination from nearby reflections in the analyser.

(b) We installed a new copper "organ-pipe" analyser, described elsewhere in these proceedings[4], which gave intensity increases of a factor 3 to 5.

(c) The detector complement was increased further from 64 to 96. The angular range now covered is from 7° to 62°.

(d) The line-up detector system was modified so that the three detectors now have independent preamplifiers and independent channels in the multiplexer. Summing is now done in software, although the signals can also be added directly and fed to a rate meter and simple counting chain for manual alignment of samples.

(e) Some improvements were made to the shielding in the region of the image point, mainly by using low-albedo materials (like B_4C and ^{10}B-Al) in well-engineered containers. In addition, the image point can now be flushed with argon gas.

3. Calibration procedures

By measuring Bragg peaks from a nickel powder sample at the image point, we calibrate the flight path distances as well as the initial angle and the angular increment. Further, the scattering through the analyser of a ZrH_2 powder at the sample position is a check of the initial calibration; in this case, the elastic peak should also correspond to zero energy transfer if the calibration is correct.

The above procedure was further tested by running with a KBr powder at the sample position using the 220 reflection in Ge for analysing the final energy of the neutron. In this case, the 111 Bragg reflection in KBr is within the Q-range of the instrument. It can be easily shown that the Bragg peak should appear at $Q_{||} = 0.51$ Å^{-1}. As can be seen in Fig. 1, the scattering from this sample is an ellipse centered about zero energy transfer and $Q_{||} \cong 0.5$ Å^{-1}. Thus the Q calibration of the instrument is satisfactory.

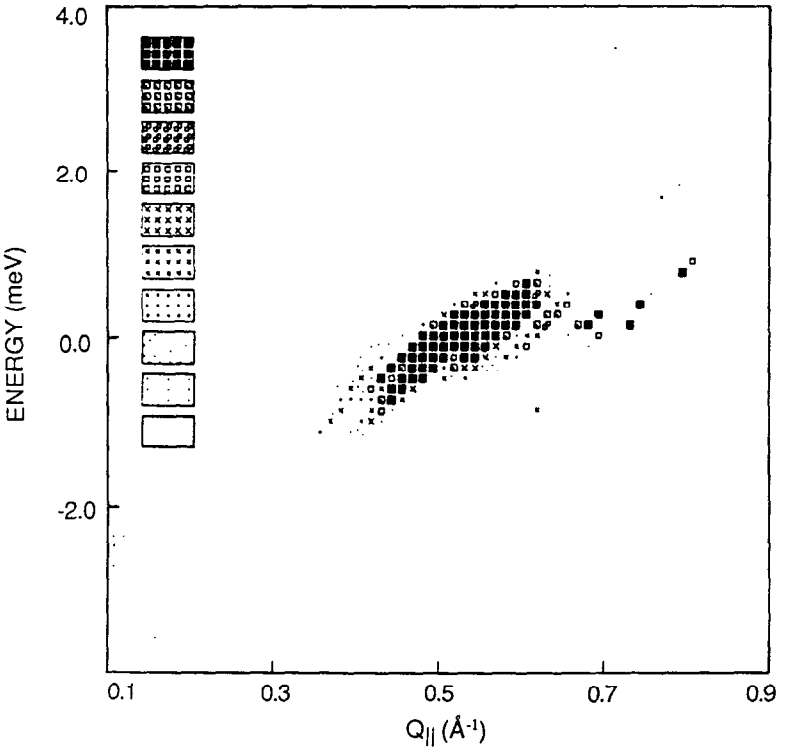

Fig. 1 The resolution of the spectrometer mapped out in the ($Q_{||}$, E) plane using a KBr powder sample and a Ge 220 analyser. The calculated peak position for the 111 Bragg peak in KBr is $Q_{||} = 0.51$Å^{-1}, E = 0. This is a good check of the momentum transfer calibration of the spectrometer.

4. Measurement of spin waves in iron[5]

Inelastic neutron scattering measurements have been made on a single crystal of Fe^{54} (12 at.% Si) that weighed ~166 gms. The spectrometer locus in Q-space for a representative run is shown in Fig. 2(a). This scan was through the 110 Bragg peak in Fe and within 10.9° of a [200] direction. Figure 2(b) indicates the available range in energy transfer as a function of $Q_{||}$. A typical time-of-flight spectrum from a

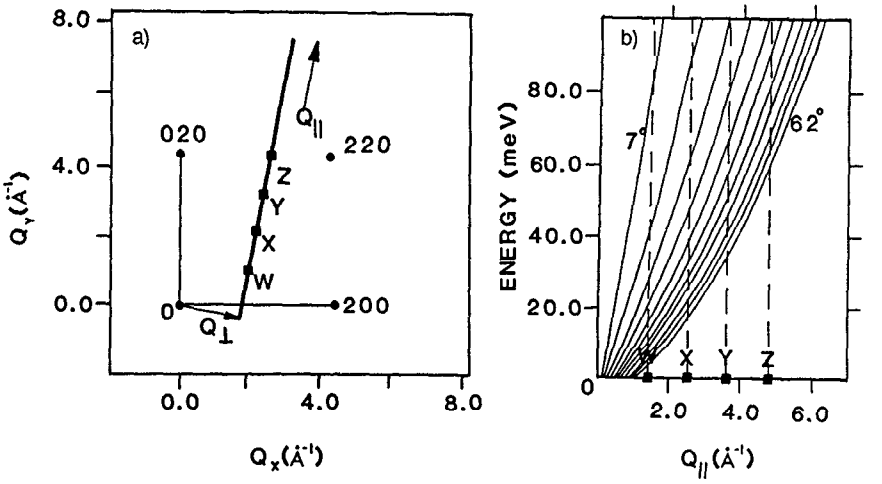

Fig. 2 The kinematics of the scan used for Fe (Cu 002 analyser). Figure 2(a) shows a section of the (hk0) zone in the reciprocal lattice of Fe. The bold line indicates the spectrometer locus along which $Q_{||}$ increases. The scan passes through the 110 reciprocal lattice point, which is marked X. Figure 2(b) shows the available energy range as a function of $Q_{||}$, for angles between 7° and 62°. The values of $Q_{||}$ marked W,X,Y and Z correspond to the points indicated in Fig. 2(a).

single detector is shown in Fig. 3. The three inelastic peaks seen in the data can be identified as the transverse acoustic phonon, the longitudinal acoustic phonon (which is unresolved from a magnon), and a second magnon mode, in order of increasing energy transfer. The individual detector scans were fitted with three Gaussians and the centers of each of the Gaussians are plotted in Fig. 4 against the corresponding value of $Q_{||}$. The dashed line is the calculated position, using the relation: $E(q) = Dq^2$ where the value of D used is 230 meV $Å^2$, which was obtained in Ref. 6. Since the system is isotropic, this relation should still be valid even though the scan is not along a high symmetry direction. A very respectable agreement between the calculated and observed values is to be noted. We point out that this analysis is preliminary and that we have presented a limited portion of the data that we have taken.

Measurements were also made at room temperature, but the background at higher energies (which is presumably due to multi-phonon scattering) was significantly reduced in the low temperature data shown here.

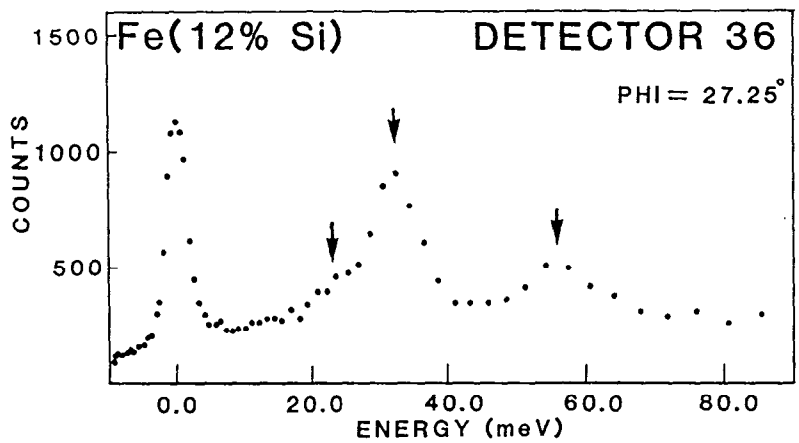

Fig. 3 A representative time-of-flight spectrum, from a single detector, for a 166-g sample ^{54}Fe (12at. % Si) at 10 K, with a Cu 002 analyser. This scan, which took three days to run, corresponds to the configuration shown in Fig. 2. Three inelastic features can be seen and these are marked by arrows. The excitation at approximately 55 meV is a magnon, which corresponds to $Q_{||} = 3.0$ Å^{-1}.

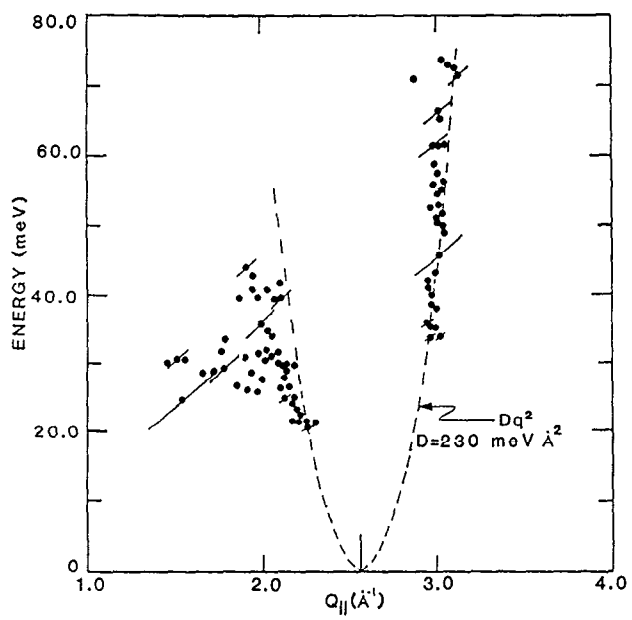

Fig. 4 The dispersion curve obtained for Fe from scans like the one shown in Fig. 3. The inelastic peaks were fitted with Gaussians and the centers of these Gaussians are plotted here against the corresponding $Q_{||}$. The dashed line represents the parabolic spin wave dispersion measured previously by Lynn[6]; (D = 230 meV Å^2). The spin wave branch on the right is well resolved, but that on the left is poorly resolved from low-lying phonons, as can be seen in Fig. 3.

5. Graphite

We have also made a study of phonons in pyrolytic graphite. The spectrometer locus in Q-space for a representative run is shown in Fig. 5(a). This scan was through the 005 Bragg peak and 31.7° away from the [001] direction. Figure 5(b) indicates the available range in energy transfer as a function of $Q_{||}$. A typical time-of-flight spectrum from a single detector is shown in Fig. 6.

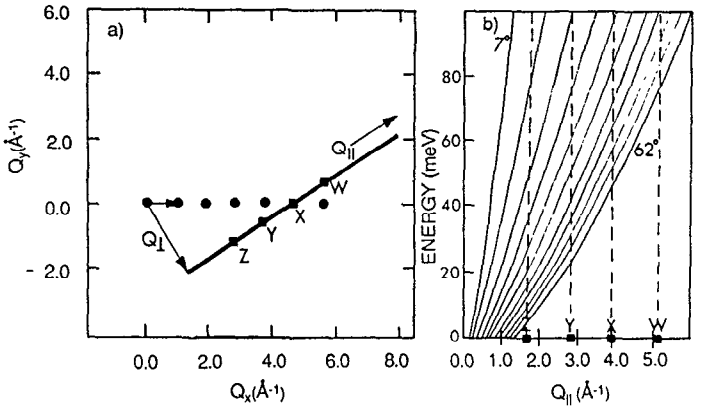

Fig. 5 The kinematics of the scan used for graphite (Cu 220 analyser). Figure 5(a) shows a section of the reciprocal lattice of graphite. The bold line indicates the spectrometer locus along which $Q_{||}$ increases. The scan direction is along this line, where the point marked X is the 005 Bragg reflection. Q_x is along the c* axis and Q_y is in the basal plane of the sample. Figure 5(b) shows the available energy range as a function of $Q_{||}$, for angles between 7° and 62°. The values of $Q_{||}$ marked W,X,Y and Z correspond to the points indicated in Fig. 5(a).

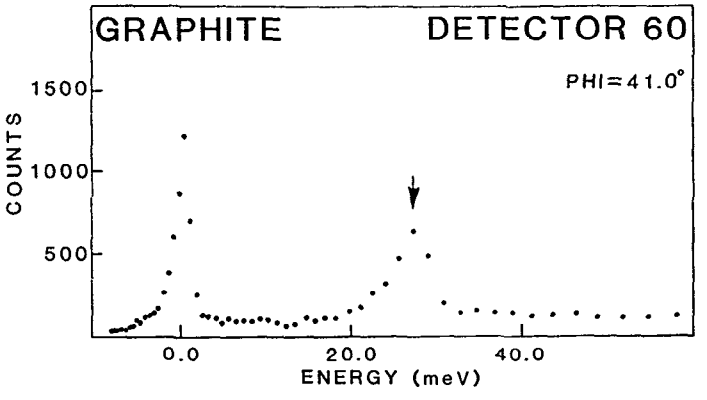

Fig. 6 A representative time-of-flight spectrum, from a single detector, for a sample of pyrolytic graphite with a Cu (220) analyser. This scan, which took two days to run, corresponds to the configuration shown in Fig. 5. A phonon can be seen at approximately 28 meV, which corresponds to $Q_{||} = 2.16$ Å^{-1}.

A phonon can be seen clearly at approximately 28 meV. By finding the center of the peak and plotting the energy against the corresponding Q-vector, a dispersion curve is obtained. In addition, by looking at the contribution of each detector in any given energy window and normalising the intensity against the ZrH_2 elastic peak intensity, detector by detector, constant-E scans can be obtained. An example of a constant-E scan at E = 28 meV is shown in Fig. 7. The dispersion curve resulting from a series of constant-energy scans between 20 meV and 40 meV (with 2meV bandwidths) is shown (open circles) in Fig. 8, as is the dispersion relation obtained directly from individual detector peaks (dots). It should be noted that this is a preliminary analysis. Again, this is part of a more extended study of the phonons in graphite, but we have not yet had time to complete the full analysis.

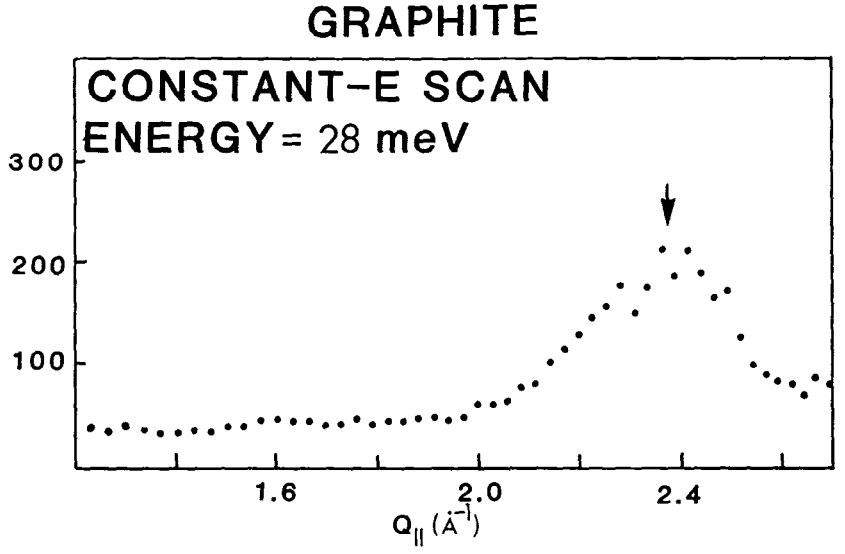

Fig. 7 A constant-E scan for the configuration shown in Fig. 5. This scan was obtained from raw data, like that shown in Fig. 6, with an energy transfer of 28 (± 1) meV. The peak is centered at $Q_{||} \cong 2.35$ Å^{-1}. This procedure was carried out for several different energies and the results can be seen in Fig. 8.

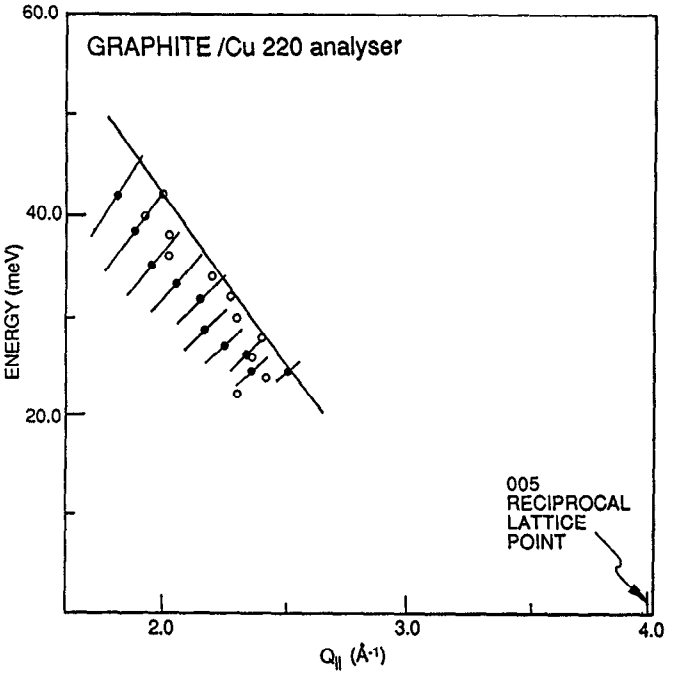

Fig. 8 The dispersion curve for graphite obtained from the scan described in Fig. 5. The solid circles represent peaks in time-of-flight scans and the open circles were obtained from constant-E scans, like that shown in Fig. 7. It can be seen that the agreement between the two is well within the estimated error. The 005 reciprocal lattice point lies at $Q_{||} = 3.98$ Å^{-1}. The solid line shows the dispersion curve for the [110] transverse acoustic phonon branch as measured by Nicklow et al.[7].

6. Conclusions

There are a number of fundamental features of this type of spectrometer that we have found troublesome and which may severely limit its usefulness.

(a) Firstly, the fact that the scattering angle is tied to the analyser Bragg angle is very constraining. The only choice one has in reaching a given momentum transfer $\hbar Q$ is in the choice of analyser d-spacing. This gives one very little latitude in manipulating the resolution function to obtain focusing. This constraint is peculiar to the constant-Q geometry and does not apply to the other pulsed-source crystal analyser spectrometer, the high-symmetry spectrometer[7], which has one more degree of freedom in its operation.

(b) Secondly, even for constant-energy transfers, the energy resolution varies as a function of scattering angle. This is because the analyser Bragg angle (and therefore E_F) vary with scattering angle. This is also true in the high-symmetry configuration[8], but is not for conventional constant-E_I machines (like chopper spectrometers) or reactor triple-axis spectrometers.

(c) Thirdly, the sample-analyser distance is relatively small (20 cm) in our case, even with a very large analyser array. While vertical collimation can be installed fairly readily in this section of the spectrometer, it is impossible to include divergent horizontal collimation without severely reducing the amount of sample viewed by the analyser, with a consequent unacceptable loss in intensity. This means that the shielding in this part of the spectrometer is weak and that background levels are higher than in spectrometers with well-collimated beams everywhere. This problem is peculiar to the constant-Q geometry.

On the other hand, the surface on which the constant-Q spectrometer measures is a simple one, in contrast to that for constant-E_I machines (see Fig. 1 of Ref. 2). Even though the latter appear to give better signal-to-noise ratios, it is not yet clear whether single crystal data taken on them can really be analysed.

References

1. C. G. Windsor, R. K. Heenan, B. C. Boland and D. F. R. Mildner, 1978, Nucl. Instrum. Methods 151, 477.
2. R. A. Robinson, R. Pynn and J. Eckert, 1985, Nucl. Instrum. Methods A241, 312.
3. R. A. Robinson, R. Pynn, J. Eckert and J. A. Goldstone, 1985, in Proceedings of VIIIth meeting of ICANS, Oxford 8-12th July 1985, Rutherford-Appleton Laboratory Report RAL-85-110 Vol.II, p.600.
4. M. Yethiraj and R. A. Robinson, 1988, in these proceedings. Los Alamos preprint LA-UR-88-3060.
5. M. Yethiraj, R. A. Robinson, J. W. Lynn and H. A. Mook, to be published.
6. J. W. Lynn, 1975, Phys. Rev. B11 , 2624.
7. R. Nicklow, N. Wakabayashi and H. G. Smith, 1972, Phys. Rev. B5 , 4951.
8. K. Tajima, Y. Ishikawa, K. Kanai, C. G. Windsor and S. Tomiyoshi, 1982, Nucl. Instrum. Methods 201, 491.